A Preliminary Modeling and Control Framework for a Hybrid UAV J-Lion

Yijie Ke*, Kangli Wang, and Ben M. Chen
Unmanned System Research Group,
Department of Electrical and Computer Engineering, National University of Singapore, Singapore 117582

ABSTRACT

J-Lion is a tail-sitter UAV platform developed to perform both VTOL and cruise flight missions. This paper presents a preliminary modeling and control framework for our hybrid UAV J-Lion. A unified model structure including comprehensive model components is derived for full envelop flight conditions. Currently, model-based controller has been specifically designed for V-TOL mode that can handle large angle deviations. Our method is verified by outdoor flight tests with existence of strong wind gust.

NOMENCLATURE

δ_p	Vectoring thrust angle in pitch channel. Positive value means that vectoring thrust propellers produce positive pitch torque
$\delta_{\text{fin1}}, \delta_{\text{fin2}}$	Deflection angles of two fins. Positive value means that fin deflection produces positive pitch torque
ω_1, ω_2	Rotating speed of two propellers
ϕ, θ, ψ	Euler angle
ρ	Air density
$\boldsymbol{\Omega}_b$	Vector of angular velocities expressed in body frame
$\boldsymbol{F}_{\text{aero}}$	Aerodynamic force expressed in inertial frame
$\boldsymbol{F}_{\text{fin\_b}}$	Drag force vector from fins expressed in body frame
$\boldsymbol{F}_{\text{surface}}$	Forces from control surfaces and fins expressed in inertial frame
$\boldsymbol{M}_{\text{aero}}$	Aerodynamic torque expressed in body frame
$\boldsymbol{M}_{\text{prop\_gyro}}$	Gyroscopic torque from rotating propellers expressed in body frame
$\boldsymbol{M}_{\text{prop}}$	Torque from rotating propellers expressed in body frame
$\boldsymbol{M}_{\text{surface}}$	Torque from control surfaces and fins expressed in body frame
$\boldsymbol{M}_{\text{vectorT}}$	Torque from vectoring thrust effect expressed in body frame
$\boldsymbol{R}_{\text{BE}}$	Rotation matrix from body frame to inertial frame
$\boldsymbol{r}_{\text{prop}}$	Vector from CG to center of propeller center, expressed in body frame
$\boldsymbol{R}_{\text{RB}}$	Rotation matrix from rotor frame to body frame
A_{prop}	Area of propeller actuator disk
AR_{fin}	Aspect ratio of two fins
e	Oswald efficiency factor, usually set to be between 0.7 and 0.85 [6]
g	Gravity acceleration
I_f	Moment of inertia matrix in diagonal form
$J_{\text{prop1}}, J_{\text{prop2}}$	Moment of inertial of two propellers
$M_{\text{prop1}}, M_{\text{prop2}}$	Torque from two rotating propellers
p, q, r	ngular velocity along three body axes
q_0, q_1, q_2, q_3	Quaternion elements, where q_0 is scalar part, and (q_1, q_2, q_3) is vector part
r_{fin}	Distance between CG and fin center in y_b axis direction
$Re_{\text{fin}i}$	Local Reynolds number of two fins in slipstream
S_{fin}	Single fin area
T	Total thrust from two propellers
u, v, w	Velocities expressed in inertial frame
V_∞	Axial inflow speed for two propellers
$V_{\text{slip1}}, V_{\text{slip2}}$	Slipstream velocity for two fins

*Email address: keyijie@u.nus.edu

1 Introduction

Hybrid UAV, which combines the advantages of VTOL and cruise flight capabilities, is a design concept that can meet the requirement of missions in both open and clustered environments, and it's an attractive solution for applications with multiple flight envelopes that cannot rely merely on fixed-wing or rotorcraft UAVs. Design examples can be referred in [1–3].

In the view of system integration, development of a hybrid UAV platform is an iterative multidisciplinary process consisting of mechanical design, aerodynamics, system-on-chip, software and algorithm design. And the modeling and control framework plays a key role in the development cycle in order to modularly integrate various design elements such as modeling components, advanced flight control algorithms, and onboard flight health monitoring, etc.

Therefore, this paper will present a preliminary modeling and control framework for hybrid UAVs. A unified model structure will be derived to account for full AOA (angle of attack) envelop flight dynamics. Control design can then be carried out based on those model components in different flight conditions.

The paper is organized as followed: Section 2 will introduce briefly our hybrid UAV platform J-Lion. Section 3 will give the derivation of unified model structure. Section 4 will specifically cover the control design for VTOL mode based on proposed model structure. Implementation and results will be presented in Section 5 to verify our method. Conclusions are finally made in Section 6 with future work illustration.

2 Platform

J-Lion is a hybrid UAV with tail-sitter configuration developed in NUS. The design methodology follows the approach in previous work [4]. The picture of real platform is shown in figure 1, and main components are illustrated below:

(1) Propeller:

Two propellers driven by brushless DC motors provide the thrust for J-Lion, and vectoring thrust is realized by using one DOF (degree of freedom) gimbal mechanism. The propellers can also provide pitch torque and differential thrust for pitch and roll stabilization.

(2) Fin:

Two fins are designed in the slipstream of propellers to enable yaw control in VTOL mode, and also enhance pitch control during transition.

(3) Control surfaces:

Same with conventional fixed-wing UAVs, elevator, aileron and rudder control surfaces are designed.

(4) Electronics:

Pixhawk autopilot is chosen as our main electronics device, together with various servos, GPS, and other sensors such as airspeed sensor. Note that the airspeed sensor data is utilized for transition and cruise flight only.

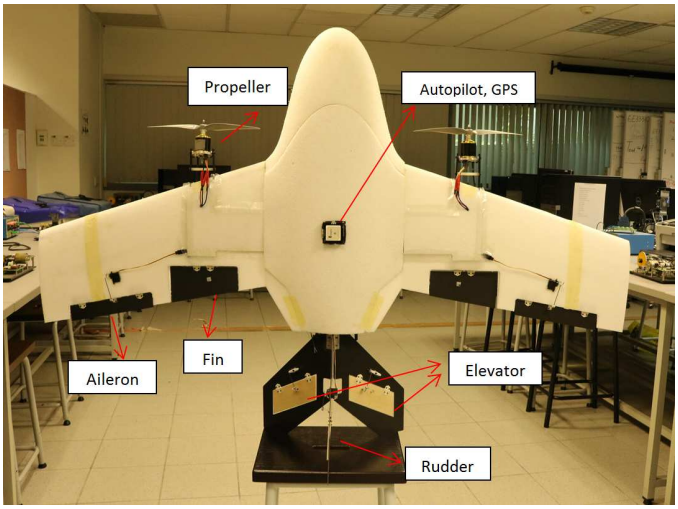

Figure 1: J-Lion platform

3 Model structure

A unified model structure is advantageous in the sense that the structure is tailorable depending on flight conditions. For example, the fins provide yaw control torque during VTOL mode by deflecting in opposite directions, while they can also provide torque for pitch control in transition by deflecting in the same direction. A unified model can greatly ease mode-switching difficulties because flight modes sometimes have no clear boundaries during flight maneuvers.

Our model structure consists of three parts: kinematics equation, force equation and moment equation. Various components can be integrated into the structure based on whether they are in our interests or not, such as vectoring thrust torque, aerodynamic lift and drag in fixed-wing mode, etc.

3.1 Coordinate frames

Shown in figure 2 , three coordinate frames are defined.

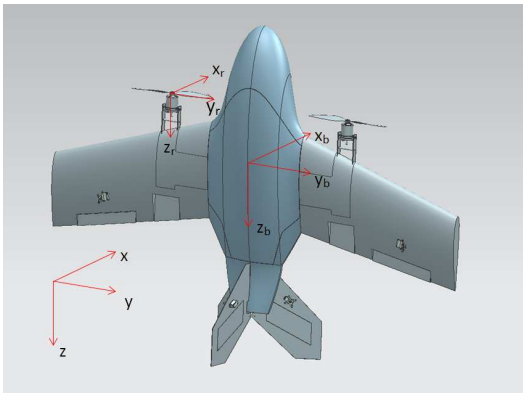

Figure 2: Coordinate frames

(1) Global inertial frame x, y, z is set to be NED frame.

(2) Body frame x_b, y_b, z_b is defined with its origin located at center of gravity (CG), and y_b, z_b direction pointing to its wingtip and tail respectively.

(3) Rotor frame x_r, y_r, z_r is also defined to describe the vectoring thrust direction. It is aligned with the body frame when no vectoring thrust angle is applied. The origin of rotor plane frame is located at the center of vectoring thrust mechanism.

3.2 Kinematics equation

The kinematics equation can be represented in Euler angle, rotation matrix or quaternion. Choosing which form to use depends on the control algorithm we'd like to use. Note that Euler angle form has intrinsic singularity problem.

1. Euler angle form

$$\begin{pmatrix}\dot{\phi}\\ \theta\\ \psi\end{pmatrix} = \begin{pmatrix}1 & \sin\phi\tan\theta & \cos\phi\tan\theta\\ 0 & \cos\phi & \text{-}\sin\phi\\ 0 & \sin\phi/\cos\theta & \cos\phi/\cos\theta\end{pmatrix}\begin{pmatrix}p\\ q\\ r\end{pmatrix} \quad (1)$$

2. Rotation matrix form

   The following strapdown equation holds:

$$\dot{\boldsymbol{R}}_{\text{BE}} = \boldsymbol{R}_{\text{BE}}\boldsymbol{\Omega}(\boldsymbol{\omega}) \quad (2)$$

   where $\Omega(\boldsymbol{\omega})$ is the skew symmetric matrix using angular velocity vector in body frame.

3. Quaternion form The differential form of quaternion is:

$$\begin{pmatrix}\dot{q_0}\\ q_1\\ q_2\\ q_3\end{pmatrix} = -\frac{1}{2}\begin{pmatrix}0 & p & q & r\\ -p & 0 & -r & q\\ -q & r & 0 & -p\\ -r & -q & p & 0\end{pmatrix}\begin{pmatrix}q_0\\ q_1\\ q_2\\ q_3\end{pmatrix} = -\frac{1}{2}\boldsymbol{\Omega_q}\mathbf{q} \quad (3)$$

3.3 Force equation

Let the position be $\boldsymbol{p} = (x, y, z)^{\text{T}}$, velocity be $\boldsymbol{v} = (u, v, w)$, the force equation is:

$$\begin{aligned}\begin{pmatrix}\dot{x}\\ y\\ z\end{pmatrix} &= \begin{pmatrix}u\\ v\\ w\end{pmatrix}\\ \begin{pmatrix}\dot{u}\\ v\\ w\end{pmatrix} &= \begin{pmatrix}0\\ 0\\ g\end{pmatrix} + \frac{1}{m}\boldsymbol{R}_{\text{BE}}\boldsymbol{R}_{\text{RB}}\begin{pmatrix}0\\ 0\\ -T\end{pmatrix} + \frac{1}{m}\boldsymbol{F}_{\text{surface}} + \frac{1}{m}\boldsymbol{F}_{\text{aero}}\end{aligned}$$

where $\boldsymbol{F}_{\text{surface}}$ refers to the forces produced by control surfaces and fins expressed in inertial frame, and the magnitude of the force is usually much smaller than others, and $\boldsymbol{F}_{\text{aero}}$ refers to the aerodynamic forces produced by the relative motion between UAV and surrounding air. In fixed-wing mode, $\boldsymbol{F}_{\text{aero}}$ is the main term in force equation.

The compact form is:

$$\begin{aligned}\dot{\boldsymbol{p}} &= \boldsymbol{v}\\ \dot{\boldsymbol{v}} &= g\boldsymbol{e_3} - \frac{1}{m}\boldsymbol{R}_{\text{BE}}\boldsymbol{R}_{\text{RB}}T\boldsymbol{e_3} + \frac{1}{m}\boldsymbol{F}_{\text{surface}} + \frac{1}{m}\boldsymbol{F}_{\text{aero}} \quad (4)\end{aligned}$$

where $\boldsymbol{e_3} = (0, 0, 1)^{\text{T}}$.

At current stage, we assume that two propellers have the same vectoring angle during flight, then R_{RB} is expressed below:

$$\boldsymbol{R}_{\text{RB}} = \begin{pmatrix}\cos\delta_p & 0 & \sin\delta_p\\ 0 & 1 & 0\\ -\sin\delta_p & 0 & \cos\delta_p\end{pmatrix}$$

3.4 Moment equation

Based on D'Alembert-Lagrange equation, the compact form of moment equation in body frame can be formulated as:

$$\begin{aligned}\boldsymbol{I_f}\dot{\boldsymbol{\Omega}}_b = -\boldsymbol{\Omega}_b \times (\boldsymbol{I_f}\boldsymbol{\Omega_b}) + \boldsymbol{M}_{\text{prop\_gyro}} + \boldsymbol{M}_{\text{surface}} + \boldsymbol{M}_{\text{prop}}\\ +\boldsymbol{M}_{\text{vectorT}} + \boldsymbol{M}_{\text{aero}} \quad (5)\end{aligned}$$

$\boldsymbol{M}_{\text{prop\_gyro}}$ is the gyroscopic torque from two propellers and the magnitude is small. $\boldsymbol{M}_{\text{surface}}$ is the torque produced by control surfaces and fins. In VTOL mode, the main component comes from fins for yaw control. In fixed-wing mode, all torques produced by control surfaces should be taken into account. $\boldsymbol{M}_{\text{prop}}$ is the torque produced by propellers which is effective in all flight conditions. $\boldsymbol{M}_{\text{vectorT}}$ is the torque from vectoring thrust which is also effective all the time. $\boldsymbol{M}_{\text{aero}}$ is the aerodynamic torque which is significant during transition and fixed-wing flight.

The expressions of those components consistent through full envelope flight are derived as:

$$\begin{aligned}\boldsymbol{M}_{\text{prop\_gyro}} &= -\begin{pmatrix}p\\ q\\ r\end{pmatrix} \times \left[\boldsymbol{R}_{\text{RB}}\begin{pmatrix}0\\ 0\\ J_{prop1}\omega_1 - J_{prop2}\omega_2\end{pmatrix}\right]\\ \boldsymbol{M}_{\text{prop}} &= \boldsymbol{R}_{\text{RB}}\begin{pmatrix}0\\ 0\\ M_{\text{prop2}} + J_{\text{prop2}}\dot{\omega_2} - M_{\text{prop1}} - J_{\text{prop1}}\dot{\omega_1}\end{pmatrix}\\ \boldsymbol{M}_{\text{vectorT}} &= \boldsymbol{r}_{\text{prop}} \times \left[\boldsymbol{R_{RB}}\begin{pmatrix}0\\ 0\\ -T\end{pmatrix}\right]\end{aligned}$$

4 CONTROL DESIGN IN VTOL MODE

Based on the model structure in previous section, we can perform control design with the consideration of corresponding model components for various flight conditions. Here, we will design specifically for VTOL mode with rotation matrix representation. First, the model components effective in VTOL mode will be derived. Position control and attitude control layers are then designed respectively as outer-loop and inner-loop.

4.1 Model components in VTOL mode

Referring to force and moment equations 4 and 5, the model components in VTOL mode are:

1. Total thrust from propellers T

$$\begin{aligned} T &= T_1 + T_2 \\ &= a_t\omega_1^2 + b_t + a_t\omega_2^2 + b_t, \end{aligned} \tag{6}$$

where a_t, b_t are propeller thrust coefficients that can be determined by experiment.

2. Forces from control surfaces and fins $\boldsymbol{F}_{\text{surface}}$

The main component of $\boldsymbol{F}_{\text{surface}}$ is the drag force from two fins, hence is with the form below:

$$\boldsymbol{F}_{\text{surface}} = \boldsymbol{R}_{\text{BE}} \begin{pmatrix} 0 \\ 0 \\ F_{\text{fin\_b}} \end{pmatrix}$$

Using propeller momentum theory [5], the drag force $F_{\text{fin\_b}}$ in body frame is:

$$F_{\text{fin\_b}} = \frac{1}{2}\rho V_{\text{slip1}}^2 S_{\text{fin}} C_{\text{Dfin1}} + \frac{1}{2}\rho V_{\text{slip2}}^2 S_{\text{fin}} C_{\text{Dfin2}} \tag{7}$$

where

$$\begin{aligned} V_{\text{slip}i} &= \sqrt{V_\infty^2 + \frac{2T_i}{\rho A_{\text{prop}}}} \\ C_{\text{Dfin}i} &= 2 * 0.074 Re_{\text{fin}i}^{-1/5} + \frac{C_{\text{Lfin}i}^2}{\pi e AR_{\text{fin}}} \\ C_{\text{Lfin}i} &= 2\pi|\delta_{\text{fin}i}| \end{aligned}$$

for $i = 1, 2$.

Note that $C_{\text{Lfin}i}, C_{\text{Dfin}i}$ are estimated using flat plate assumption, and the drag force consists of friction drag and induced drag [6]. The propeller inflow velocity V_∞ is assumed to be zero in VTOL mode.

3. Torque from control surfaces and fins $\boldsymbol{M}_{\text{surface}}$

The main component of $\boldsymbol{M}_{\text{surface}}$ is the torque produced by two fins for yaw control, hence it's with the form:

$$\boldsymbol{M}_{\text{fin}} = \begin{pmatrix} 0 \\ 0 \\ M(\delta_{fin}) \end{pmatrix}$$

We assume here that the deflection angles of two fins are the same but in opposite directions, then the $M(\delta_{fin})$ is computed as:

$$M(\delta_{fin}) = \pi\delta_{\text{fin}}\rho(V_{\text{slip1}}^2 + V_{\text{slip2}}^2)S_{\text{fin}}r_{\text{fin}} \tag{8}$$

where δ_{fin} is the fin deflection angle following torque positive sign convention.

4.2 Outer-loop design

The position control layer consists of two parts. Firstly, the velocity reference is obtained using P-control scheme with position error:

$$\boldsymbol{v_{ref}} = K_{p1\_p}\boldsymbol{e_p} = K_{p1\_p}(\boldsymbol{p_{ref}} - \boldsymbol{p}) \tag{9}$$

where K_{p1_p} is the control gain, $\boldsymbol{p_{ref}}$ is the reference position.

Then desired thrust vector can be obtained in the second part with velocity information:

$$\boldsymbol{T_d} = K_{p2\_v}\boldsymbol{e_v} + K_{d2\_v}\frac{d}{dt}\boldsymbol{e_v} + K_{i2\_v}\int \boldsymbol{e_v}dt \tag{10}$$

where $K_{p2\_v}, K_{d2\_v}, K_{i2\_v}$ are velocity control gains, $\boldsymbol{e_v}$ is the velocity error vector.

Due to thrust saturation, the desired thrust is scaled within feasible range:

$$\boldsymbol{T_{dnew}} = \frac{\boldsymbol{T_d}}{|\boldsymbol{T_d}|}sat(|\boldsymbol{T_d}|, T_{max}) \tag{11}$$

where T_{max} is the maximum thrust available from propellers, $sat()$ is the saturation function.

With the desired thrust vector, we can achieve the desired $\boldsymbol{z_b}$ vector which is aligned with $\boldsymbol{T_d}$. The desired $\boldsymbol{y_{bd}}$ vector is computed using desired yaw angle ψ_d as:

$$\boldsymbol{y_b} = (-\sin\psi_d, \cos\psi_d, 0)^{\text{T}} \tag{12}$$

Thus the rotation matrix for desired attitude can be constructed based on desired body-axis vectors. The rotation matrix will be passed to inner-loop for attitude control.

4.3 Inner-loop design

The attitude control adopts the method from [7, 8], and the control scheme consists of two loops. Loop 1 is a simple P control loop to generate the attitude rate reference, while Loop 2 uses PID control law to generate required control torque in three body axes.

• Loop 1

In Loop 1, there are two routes that account for large and small angle deviations. The Z body axis vector is obtained from the third column of rotation matrix, which is expressed in inertial frame. The control algorithm itself follows the Euler sequence used in [7] which is roll-pitch-yaw sequence.

When the deviation angle between current $\boldsymbol{z_b}$ and desired $\boldsymbol{z_b}$ is less than 90 degrees, called ROUTE 1, the algorithm will first compute roll and pitch angle error because yaw channel response is slower. The roll and pitch motion can be seen as a rotation that can transform current Z body axis $\boldsymbol{Z_b}$ to desired Z body axis $\boldsymbol{Z_{br}}$, and the minimum distance movement is determined by the coplar of $\boldsymbol{Z_b}$ and $\boldsymbol{Z_{br}}$. Hence, the euler axis $\vec{n}$ and rotation angle θ can be obtained as:

$$\vec{n} = \frac{\boldsymbol{Z}_b \times \boldsymbol{Z}_{br}}{|\ \boldsymbol{Z}_b \times \boldsymbol{Z}_{br}\ |}$$

$$\theta = atan2(\boldsymbol{Z}_b \times \boldsymbol{Z}_{br}, \boldsymbol{Z}_b \cdot \boldsymbol{Z}_{br})$$

Then the intermediate rotation matrix is expressed as:

$$\boldsymbol{R_{rp}} = \boldsymbol{R(\theta, \vec{n})} \cdot \boldsymbol{R}$$

where $R(\theta, \vec{n})$ is the rotation matrix constructed from $\vec{n}$ andθ, R is current rotation matrix.

Roll and pitch angle errors are computed by projecting the rotation angle θ to current x_b, y_b axes, and yaw angle error is less weighted and computed with the deviation between R_{rp} and R_{ref}.

Similarly, when the absolute value of deviation angle between current $\boldsymbol{z_b}$ and desired $\boldsymbol{z_b}$ is greater than 90 degrees (ROUTE 2), the algorithm computes all three angle errors simultaneously using the projection of θ to current body axes.

The angle errors are finally computed by fusing the results from ROUTE 1 and 2 together, and the angular rate references can then be computed using a simple P control scheme.

• Loop 2

With the angular rate obtained from Loop 1, PID control scheme can be used to obtain desired control torque in three body axes. Using pitch channel as an example, the desired torque in pitch channel can be computed as:

$$M_{pitch} = K_p \boldsymbol{e_{\dot{\theta}}} + K_d \frac{d}{dt} \boldsymbol{e_{\dot{\theta}}} + K_i \int \boldsymbol{e_{\dot{\theta}}} dt \qquad (13)$$

where $\boldsymbol{e_{\dot{\theta}}} = \dot{\theta}_d - \dot{\theta}$ is the angular rate error.

Note that the gains in Loop 1 and 2 can be determined with typical LQR method for certain performance requirement, and also be tuned to satisfy the torque limit from actuators expressed in moment equation 5.

5 Implementation and Results

5.1 Implementation

Our modeling and control framework is implemented in opensource PX4 software environment. The main modules involved are shown in figure 3.

Except the outer-loop and inner-loop layers, navigator module manages flight mission control, and provides position reference. In the actuator layer, the actuator inputs are calculated with actuator models, for example, throttle input for motor ESC (electrical speed controller) is computed with fitting relationship of rotating speed to throttle that is determined from experiment, and deflection of fins is computed using equation 8 to realize desired yaw control torque.

5.2 Flight results

Both semi-auto and full-auto flights in VTOL mode were conducted for J-Lion with proposed framework. In semi-auto flight, attitude references are generated by human pilot with a transmitter, and only inner-loop controller is activated. In full-auto flight, J-Lion is required to perform fully autonomous flight through several waypoints.

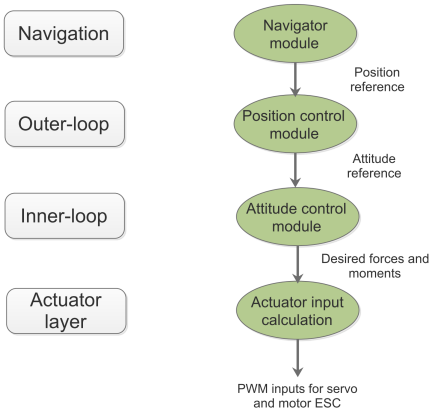

Figure 3: Framework implementation schematics

(1) Semi-auto test

The semi-auto test was conducted in indoor environment. Attitudes are plotted via their references, as shown in figures 4. From the results, we can see that the attitude stabilization of J-Lion in VTOL is well achieved despite of the offset from installation and assembly.

(2) Full-auto test

The full-auto test was conducted in outdoor environment with existence of strong wind. J-Lion was required to fly through four waypoints in VTOL mode. The four waypoints are set with the same altitude. When the UAV reaches one waypoint, the yaw reference will be set in the direction pointing to the next. The attitude curves are shown in figure 5. From the figure, the maximum pitch angle can reach up to 50 deg to counter strong wind gust in pitch channel. The flight trajectory of relative horizontal position is also shown in figure 6. It's observed that the tracking performance in VTOL mode is greatly affected by strong outdoor wind gust, but the attitude stabilization is still satisfactory. The position control performance can be improved by integrating wind gust observer in the future.

6 Conclusions and Future Work

A preliminary modeling and control framework is proposed in this paper for our hybrid UAV J-Lion. The unified model structure can integrate full envelope flight dynamics which is usually derived separately in different flight modes, and it can serve as the basis for high nonlinear dynamics modeling in transition phase. Besides, model-based control design for VTOL mode is presented based on the proposed model structure. Our framework is verified by real flight tests. In the future, we will integrate the transition model into our model structure, and design unified flight control laws for all flight modes.

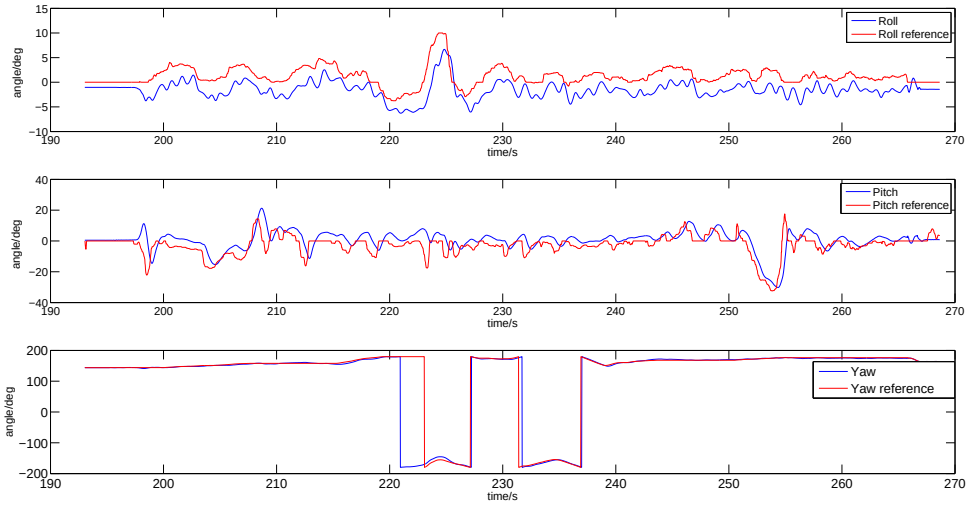

Figure 4: Attitude curve in semi-auto test

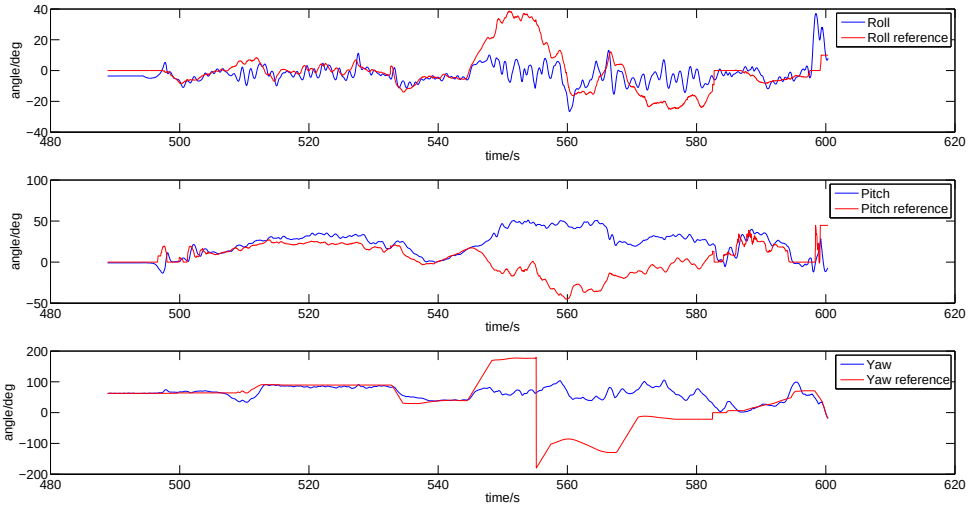

Figure 5: Attitude curve in full-auto test

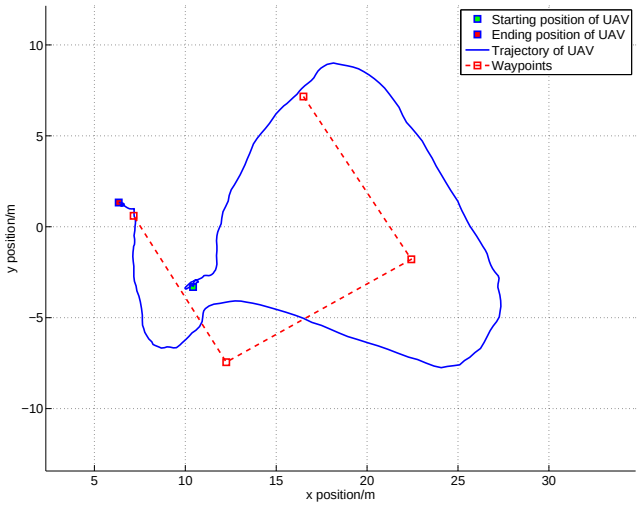

Figure 6: Flight trajectory of relative horizontal position in full-auto test

REFERENCES

[1] Kendoul, Farid, Isabelle Fantoni, and Rogelio Lozano. Modeling and control of a small autonomous aircraft having two tilting rotors. *Proceedings of the 44th IEEE Conference on Decision and Control*, 2005.

[2] Cetinsoy, E., et al., Design and construction of a novel quad tilt-wing UAV. *Mechatronics*, 22(6): p. 723-745, 2012.

[3] Stone, R. Hugh. Control architecture for a tail-sitter unmanned air vehicle. *Control Conference, 2004. 5th Asian. IEEE*, 2004.

[4] Yijie Ke, Hui Yu, Changkai Chi, Mingwei Yue and Ben M. Chen. A systematic design approach for an unconventional UAV J-Lion with extensible morphing wings. *Proceedings of the 12th IEEE International Conference on Control & Automation*, 2016.

[5] McCormick, B. W. *Aerodynamics, Aeronautics, and Flight Mechanics*. John Wiley and Sons, Inc, New York, 1995.

[6] Anderson Jr, John David. *Fundamentals of aerodynamics*. Tata McGraw-Hill Education, 2010.

[7] Mellinger, Daniel, and Vijay Kumar. Minimum snap trajectory generation and control for quadrotors. *In IEEE Conference on Robotics and Automation (ICRA)*, 2011.

[8] Lorenz Meier, Petri Tanskanen, Friedrich Fraundorfer, and Marc Pollefeys. PIXHAWK: A system for autonomous flight using onboard computer vision. *In IEEE Conference on Robotics and Automation (ICRA)*, 2011.